

A Compact, Highly Sensitive pH Sensor Based on Polymer Waveguide Bragg Grating

Nabarun Saha , Giuseppe Brunetti , Mario Nicola Armenise , and Caterina Ciminelli 

Abstract—Accurate probing, monitoring, and controlling the pH level is critical in different fields. In the last two decades, optical fiber/waveguide-based pH sensors have been widely investigated with the aim of further enhancement of sensitivity and miniaturization. Here, we propose a novel and cost-effective pH sensor based on polymer waveguide Bragg grating, addressing main aspects like sensitivity enhancement, miniaturization, narrow band response, and stable performance. The large evanescent field due to metal under cladding and high index coating combined with excellent penetration depth match with pH-sensitive polymer coating of poly-acrylic acid/poly-allylamine hydrochloride (PAA/PAH) in an aqueous medium, ensures a sensitivity of 10.4 nm/pH for a pH range of 4 to 7, two orders higher than all reported Bragg grating pH sensors to our knowledge. A narrow band (~ 1 nm) response has been ensured by low propagation loss of the TE mode. Further, the variations in sensitivity and peak reflectivity are within 3% for a $\pm 10\%$ inaccuracy in various structural parameters, reflecting excellent fabrication tolerances. The proposed sensor is an important development, especially for the perishable food industry in which a high sensitivity in a pH range of 4 to 7 is highly desirable to accurately determine the freshness of foods.

Index Terms—Gratings, photonic crystal, sensors, waveguides.

I. INTRODUCTION

REAL-TIME and in-situ detection, monitoring, and controlling the pH level are crucial in a wide range of fields like environment, agriculture, food quality control, medical diagnostics, water quality monitoring, railways, etc [1], [2], [3], [4]. In the last two decades, remarkable attention has been gained by the optical fiber/waveguide-based pH sensors over the traditional ones such as pH-electrodes and acid-based indicators, thanks to numerous beneficial features like immunity to electromagnetic interference, compactness, high sensitivity, ease of fabrication, etc. The sensitivity of optical fiber/waveguide-based sensors depends on the pH-sensitive functional layers and the enhancement of the light-analyte interaction. Based on the functional layers, these sensors can be categorized into two types, pH-indicator-based and polymeric swelling material based. For indicator-based sensors, the optical fiber/waveguide surfaces are coated with various matrix materials such as ethyl violet,

neutral red, thymol blue, acid chrome dye, etc [5], [6]. The indicator-based pH sensors often suffer from drawbacks like low self-life, instability, and source intensity fluctuations. The pH sensors based on polymeric nano-coatings are relatively new in which the polymeric thin coating like smart hydrogel [7], [8], polyvinyl alcohol/polyacrylic acid (PAA/PVA) [9], [10], Polyacrylic acid/poly-allylamine hydrochloride (PAA/PAH) [11], [12], [13] multilayers at the fiber/waveguide's surface swells or shrinks in accordance with the pH level of the surrounding medium. These polymeric coating-based sensors can overcome the aforementioned drawbacks of indicator-based sensors and also possess fast responses. The sensitivity of these sensors depends on the interaction of the evanescent field of the guided modes with the sensing medium. The enhanced interaction with the surroundings, i.e., the pH-influenced polymeric coating results in high sensitivity and thus the accurate measurement of pH. There are various pH sensors based on Bragg gratings [14], [15], [16], [17], long period gratings (LPGs) [8], [11], ring resonators [18], modal interferometers [9], [10], surface plasmon resonance (SPR) [19], [20], etc which have used different mechanisms to enhance the pH sensitivity. Among these sensors, the Bragg grating-based sensors are particularly promising due to their amenability to miniaturization, narrow band response as compared to LPG and SPR, and also unlike ring resonators and modal interferometers they can provide free spectral range (FSR) free spectrum. As a result, various pH sensors have been reported over the years with Bragg grating inscribed polymer fibers [16], micro-fiber [17], tilted grating fibers [15], etc. However, the sensitivity of the Bragg grating-based sensors is found to be on the lower side since the participating mode is well-guided within the optical fiber's core. Although the cladding of the fiber can be etched or a microfiber can be used to enhance the interacting modal field with the sensing medium, it puts the durability of optical fibers at risk. In this context, an integrated optical waveguide geometry can be an elegant solution as it provides larger freedom in choosing geometry as well as materials [21]. In the last few years, it has been reported that the evanescent field of an integrated optical waveguide can be enhanced significantly to the surrounding medium by incorporating a metal layer underneath the waveguide core [22], [23], [24]. Recently, it has been noticed that the evanescent field can be further improved by considering high-index nanocoating on top of a ridge waveguide [25]. In addition, it has been observed that the enhancement in the evanescent field is more prominent for the quasi-TE modes of the structure. Since the TE mode shows lower propagation loss as compared to the TM modes, it provides a larger possibility of

Manuscript received 21 November 2022; revised 25 January 2023; accepted 1 February 2023. Date of publication 10 March 2023; date of current version 29 March 2023. This work was supported by the Italian Ministry of University and Research under Project Monitoraggio attivo dell'infrastruttura –MAIA ARS01_00353. (Corresponding author: Caterina Ciminelli.)

The authors are with the Optoelectronics Laboratory, Politecnico di Bari, 70125 Bari, Italy (e-mail: nabarun.saha@poliba.it; giuseppe.brunetti@poliba.it; marionicola.armenise@poliba.it; caterina.ciminelli@poliba.it).

Digital Object Identifier 10.1109/JPHOT.2023.3242820

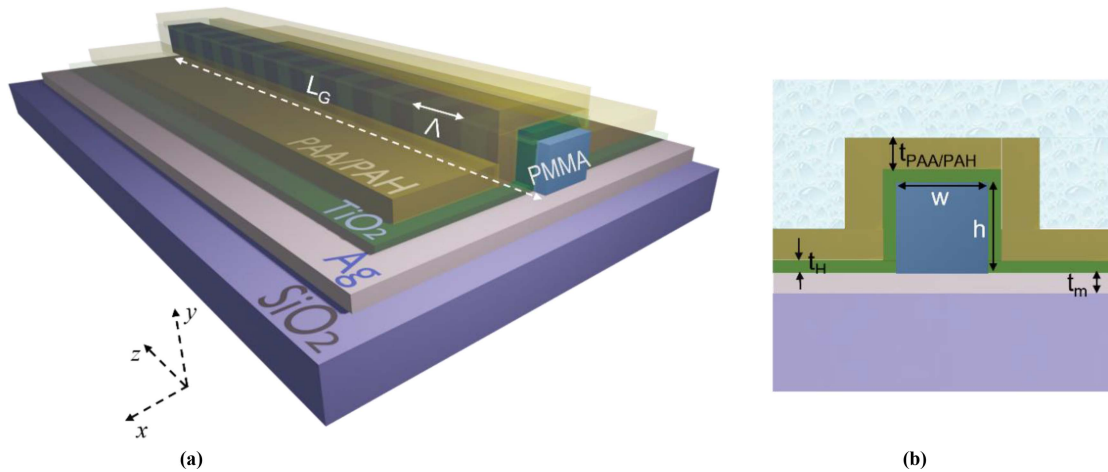


Fig. 1. (a) The 3D schematic diagram and (b) the cross-sectional view of the proposed structure. The values of the width (w) = $1.5 \mu\text{m}$, height (h) = $1.5 \mu\text{m}$, high index layer thickness (t_H) = 60 nm , metal layer thickness (t_m) = 200 nm , grating period (Λ) = 510 nm , grating length (L_G) = 0.9 mm .

obtaining a narrow band spectrum, facilitating the detection of analytes.

In this paper, utilizing the beneficial feature of metal under cladding and high index coating a highly sensitive, narrow-band, compact polymer Bragg grating-based pH sensor has been reported. The PAA/PAH polymeric coating has been used as the functional layer to sense the PH level in the aqueous medium. The thickness of the PAA/PAH layer has been chosen based on the reported results and is found to be an excellent match with the penetration depth of the evanescent field, resulting in high sensitivity. The pH sensitivity is found to be 10.4 nm/pH for a pH range of 4 to 7. Further, the 3-dB bandwidth is found to be $\sim 1 \text{ nm}$ with excellent stability in peak reflectivity for the entire pH range. The proposed sensor is an excellent match for measuring the pH level of perishable foods.

II. PROPOSED STRUCTURE AND OPERATING PRINCIPLE

The schematic of the proposed pH sensor is illustrated in Fig. 1(a) and the corresponding cross-section is in Fig. 1(b). It consists of a ridge shape polymer core waveguide made of Polymethyl methacrylate (PMMA) which is situated on top of a silver (Ag) coated fused silica substrate. The entire structure is coated with a high index layer of Titanium dioxide (TiO_2) followed by a nano-coating of PAA/PAH. The aqueous solution has been assumed as the cover medium. The metal layer underneath the core pushes the modal field towards the sensing medium due to its high negative dielectric constant and high reflectivity [22]. The high index layer of TiO_2 pulls the mode further towards the sensing medium as the guided mode is prone to move towards the high index layer [25]. As a result, the combined effect of metal under cladding and high index coating leads to the enhancement of the evanescent field in the surroundings and thus in the pH-sensitive PAA/PAH nano-coatings. The Bragg grating has been realized by considering the periodic modulation of the core refractive index which couples the forward and backward propagating fundamental mode. The modulated

and unmodulated section of the core has been represented with different blue shades in the schematic diagram.

The duty cycle of the grating is taken to be 0.5. Following the coupled mode theory (CMT), the reflected spectrum can be expressed as [22], [26],

$$R = \left| \frac{\kappa \tanh(\gamma L)}{\gamma + (\alpha + i\delta) \tanh(\gamma L)} \right|^2 \quad (1)$$

where α is the field attenuation coefficient, $\delta = (2\pi n_{00}/\lambda - \pi/\Lambda)$ is the phase mismatch factor with n_{00} being the real part of the modal effective index of the TE_{00} mode and $\gamma = \sqrt{(\kappa^2 + (\alpha + i\delta)^2)}$. In the above equation, κ is the coupling coefficient defined as [22], [25],

$$\kappa = \frac{1}{2} n_{co} w \epsilon_0 \iint \Delta n \mathbf{E} \cdot \mathbf{E} dA \quad (2)$$

where Δn is the amplitude of the refractive index modulation or the grating strength and \mathbf{E} is the power normalized electric field component. The analysis has been carried out by following the basic boundary condition, i.e., the tangential component of electric field component \mathbf{E} , and magnetic-field component \mathbf{H} should be continuous at each interface of the waveguide structure. The Finite Element Method (FEM) based tool Comsol Multiphysics has been used to study the modal properties of the structure and next the CMT has been used to estimate the spectral behavior and sensitivity of the proposed structure through Matlab coding. At the resonance ($\delta = 0$), the reflectivity becomes maximum and its position depends on the pH level of the surrounding medium. Depending upon the pH level, the pH-sensitive polymeric layer of PAA/PAH swells or shrinks. Accordingly, the modal evanescent field interacting with the PAA/PAH layer modulates the modal effective index and thus the resonance condition. As a result, the position of the peak reflectivity shifts along the wavelength axis, measuring which sensitivity has been calculated. Here we like to mention that the proposed sensor has been modelled following [11], [27] in which it has been shown that the nanolayer of PAA/PAH

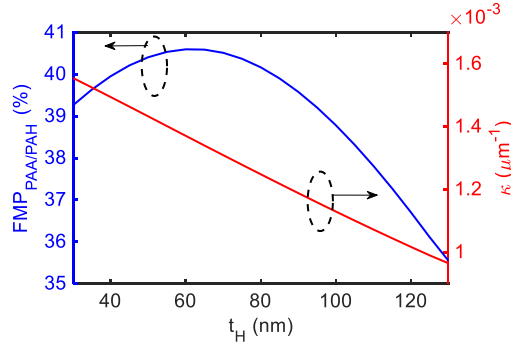


Fig. 2. Variation of FMP in the PAA/PAH and the grating coupling coefficient as a function of high index layer (TiO₂) thickness.

shrinks from 400 nm to 150 nm for a pH range of 4 to 7. As it will be discussed later, this thickness range of the PAA/PAH layer is found to be particularly promising for the proposed structure as it matches well with the penetration depth of the evanescent field. The wavelength dependency for the materials' refractive indices has been taken into account by following the corresponding Sellmeier relations [22], [28], [29] except for the silver layer. For the silver layer, Johnson and Christy's data have been considered with the cubic fit and linear fit for the real and imaginary part of the refractive indices respectively [30].

III. RESULTS AND DISCUSSIONS

A. Performance Optimization & pH Sensitivity

The core of the proposed structure is considered to have a square cross-section with a dimension ($w \times h$) of $1.5 \times 1.5 \mu\text{m}$, which supports only the fundamental mode [22]. The single-mode operation is generally preferred in Bragg grating-based structures to avoid inter-modal coupling and interference. A thickness of the metal layer (t_m) of 200 nm has been assumed to minimize the power leakage in the substrate [22], [24]. The thickness of the high index layer plays the most important role. The variation of fractional modal power (FMP) in the PAA/PAH layer and the grating coupling coefficient as a function of the high index layer's thickness t_H is plotted in Fig. 2. The thickness of the PAA/PAH is taken to be 400 nm. The FMP in the PAA/PAH nanolayer is defined as [25],

$$FMP_{PAA/PAH} = \frac{\iint_{PAA/PAH} (\mathbf{E} \times \mathbf{H}) \cdot \hat{z} dA}{\iint_{All\ Area} (\mathbf{E} \times \mathbf{H}) \cdot \hat{z} dA} \quad (3)$$

where \mathbf{E} and \mathbf{H} are the power-normalized electric and magnetic field components. As shown in Fig. 2, the FMP in the PAA/PAH layer initially increases as t_H increases up to $t_H = 60$ nm and then FMP decreases. This behaviour can be attributed to the modal property of the TE₀₀ mode. The mode is mostly guided in the PMMA core at lower thicknesses, resulting in a lower evanescent field at the PAA/PAH layer. At higher thicknesses, the mode becomes more confined in the high index layer, reducing the interacting power in the PAA/PAH layer again. The FMP in the PAA/PAH is found to be maximum around $t_H = 60$ nm. As shown in Fig. 2, at this optimum thickness almost 41% of modal power is available to interact with the

pH-sensitive layer, resulting in potential high sensitivity. It is also worth noting that the coupling coefficient is reducing as the thickness of the high index layer increases. With the increase in thickness, the TE₀₀ mode becomes more confined in the TiO₂ layer, reducing the interacting modal power with the grating inscribed PMMA core. Therefore, choosing a lower thickness of the high index layer also ensures a higher coupling coefficient. As a result, a significant peak reflectivity can be obtained with a lower grating length. Fig. 3(a) represents the cross-sectional field distribution of the TE₀₀ mode, by assuming the aforementioned features and a 400 nm thick PAA/PAH layer.

The modal field is mostly pushed towards the high index layer and a large amount of field is available to interact with the pH-sensitive layer. In order to find out the penetration depth and its compatibility with the PAA/PAH layer's thickness, the field distribution in the vertical direction corresponding to the white line in Fig. 3(a) has been plotted in Fig. 3(b) (blue graph). The evanescent field penetration depth is found to be 438 nm, which is matching well with the thickness of the PAA/PAH layer. Therefore, not only the enhancement in the evanescent field but also a large portion of the evanescent field is available to interact with the pH-sensitive layer, ensuring a high pH sensitivity. In order to point out the importance of the metal under cladding in Fig. 3(b) we have also plotted the vertical field distribution without the metal layer (grey graph). The figure clearly shows that the metal layer pushes the mode upwards from the substrate. It should be noted that in the absence of the metal layer since a significant amount of power is in the substrate, the metal layer increases the fractional modal power in the pH-sensitive PAA/PSAH layer. The FMP in the PAA/PAH layer is found to be 0.37 and 0.41 with and without the metal layer, showing an enhancement of around 10% due to the metal layer. From Fig. 3(b), it is also clear that the penetration depth of the evanescent field is decided by the high index layer.

It is to be noted that the resonance wavelength depends on two quantities, the grating period (Λ) and the modal effective index (n_{00}) of the waveguide. The two most important parameters deciding the modal effective index are the width of the core (w) having a square cross-section ($w = h$) and the thickness of the high index layer (t_H). Therefore, in order to design the grating period two graphs have been plotted in Fig. 4(a) and (b), showing the variation of resonance wavelength with the grating period for three different values of width and high index layer thickness respectively. In both cases, resonance wavelength shows a red shift with the increase in the grating period. The effect of the high index layer thickness is found to have a greater impact on the resonance wavelength as compared to the waveguide's width. The grating period is chosen to be 510 nm for $w = 1.5 \mu\text{m}$ and $t_H = 60$ nm, to have the resonance wavelength around 1550 nm. The grating length (L_G) has been optimized following the behaviour of peak reflectivity and full width at half maximum (FWHM). The variation of peak reflectivity and the FWHM has been plotted simultaneously in Fig. 5, as a function of grating length, considering a grating strength of 8×10^{-4} . The figure shows that with the increase in grating length the peak reflectivity increases whereas the FWHM decreases. Although a longer grating length can provide very high peak reflectivity and low FWHM, a compromise must be made with the device's

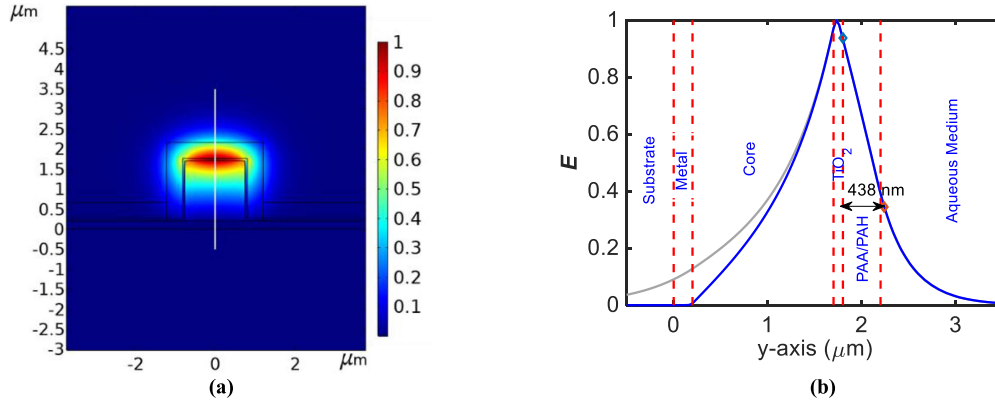


Fig. 3. (a) The modal field distribution of the TE_{00} mode. The RI of the substrate (SiO_2) = 1.444, core (PMMA) = 1.4809, high index layer (TiO_2) = 2.2914 at wavelength $1.55 \mu m$. (b) The normalized field distribution in the vertical direction individually corresponds to the white line in Fig. 3(a). The blue and grey color figure represents the field distribution with and the without metal layer. In the absence of the metal layer, in the figure, the metal layer area should also be considered as the substrate.

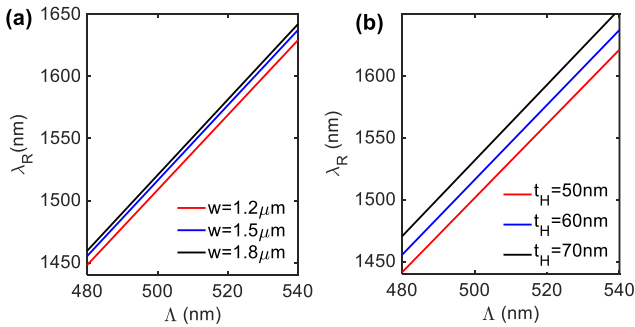


Fig. 4. Variation of resonance wavelength with the grating period for (a) three different values of waveguide's width with $t_H = 60 \text{ nm}$ and (b) three different values of high index layer's thickness with $w = 1.5 \mu m$.

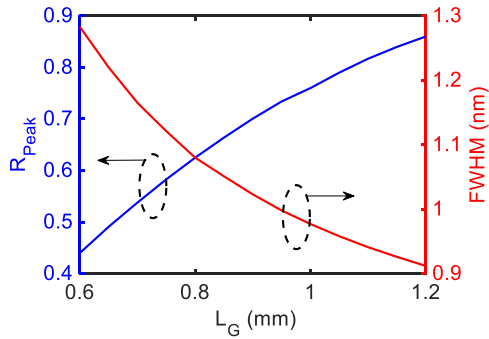


Fig. 5. Variation of peak reflectivity and full width at half maximum with the grating length.

compactness. The grating length is chosen to be 0.9 mm such that the FWHM is about 1 nm with a peak reflectivity of 0.7 . The corresponding reflected spectrum is plotted in Fig. 6, showing an FWHM = 1.02 nm and peak reflectivity = 0.7 . Since the high index layer pulls the TE_{00} mode towards it, the modal field in the metal layer reduces significantly. As a result, the propagation loss due to metallic absorption reduces significantly. The propagation loss is found to be only 1.05 dB/cm and the corresponding

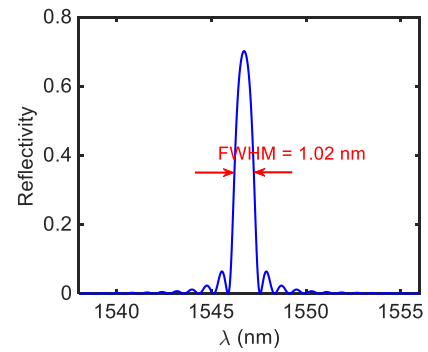


Fig. 6. The reflected spectrum for a 400 nm thick PAA/PAH nano-coating.

propagation length (length at which the modal power becomes $1/e$ of input) is found to be 41 mm . The propagation length is found to be much higher than a simple metal under-cladding structure where typically it varies between 1 to 10 mm for the TE_{00} mode [22], [23], [24]. The increment in propagation length plays an important role in obtaining narrow spectrum bandwidth of $\sim 1 \text{ nm}$.

In order to justify the waveguide grating operation, the field intensity distribution for three different wavelengths is shown in Fig. 7: two off-resonance wavelengths 1540 nm and 1555 nm and at resonance wavelength 1546.7 nm . At off-resonance wavelengths, only the field distribution related to the forward propagating mode is shown whereas both the forward and backward propagating mode is plotted for the resonance wavelength. As it can be seen at the off-resonance wavelength the field intensity of the mode remains almost constant along the direction of propagation. At the resonance wavelength, the intensity of the forward propagating mode reduces along the $+z$ -axis whereas the intensity build-up for the backward propagating mode towards the input end justifies the waveguide grating operation.

In order to estimate the pH sensitivity, the thickness of the PAA/PAH layer is varied from 400 nm to 150 nm which corresponds to a change in pH values from 4 to 7 [11], [27]. The

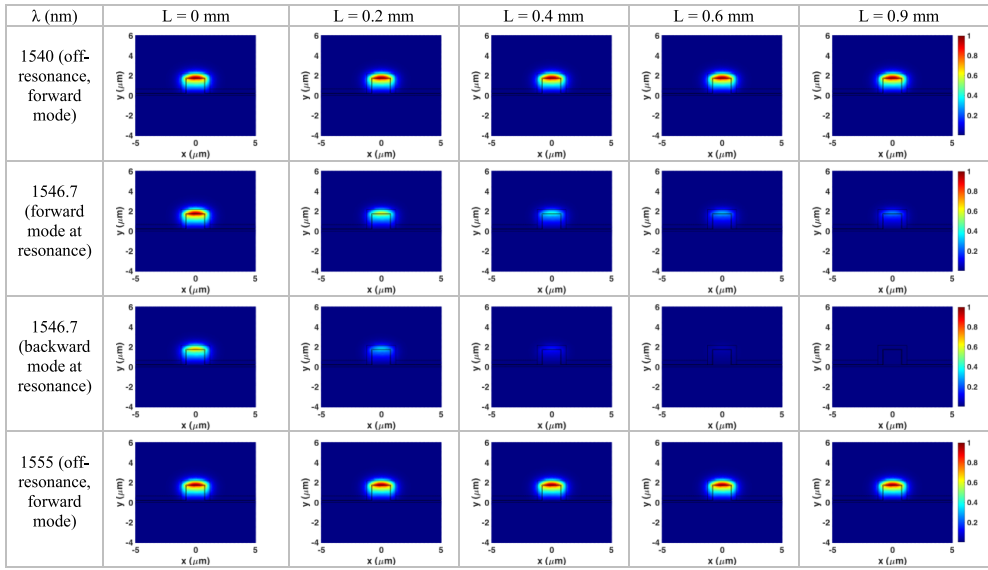


Fig. 7. The field distribution along the propagation direction at three different wavelengths. Only the forward propagating mode is shown at two off-resonance wavelengths whereas both forward and backward propagating modes are shown at the resonance wavelength.

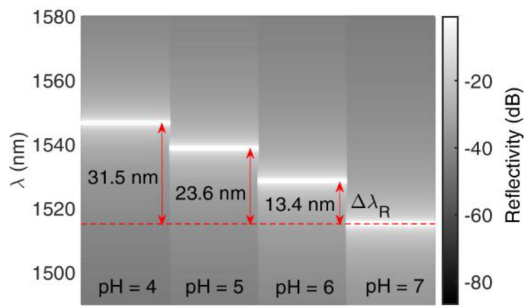


Fig. 8. The reflected spectrum for four different pH values.

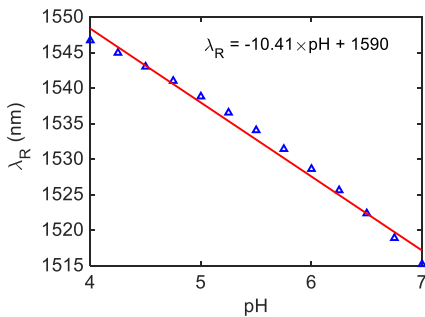


Fig. 9. The variation of resonance wavelength with different pH values.

refractive index of the PAA/PAH layer is taken to be 1.55 [11]. The reflected spectrum for four different pH values has been shown in Fig. 8 as a surface plot. The peak reflectivity is found to be stable with the change in pH. As visible in the figure, the shift in resonance wavelength ($\Delta\lambda_R$) is relatively higher near pH of 7 as compared to pH of 4. The overall shift in resonance wavelength is found to be 31.5 nm. The variation of resonance wavelength (λ_R) with the pH values has been plotted in Fig. 7 with a linear fitting having R^2 value of 0.989. The corresponding linear fitting equation is shown in the figure,

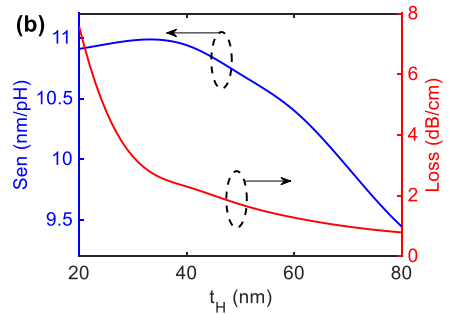
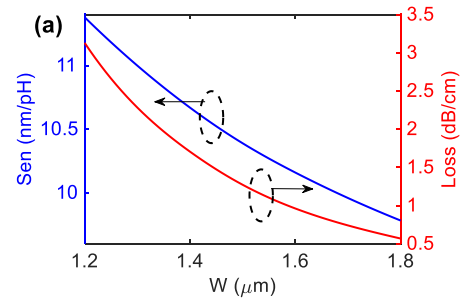


Fig. 10. Variation of pH sensitivity and propagation loss as a function of (a) waveguide's width and (b) thickness of the high index layer.

the slope of which provides the pH sensitivity, found to be 10.41 nm/pH. Considering the spectrometer resolution to be 20 pm, the detection limit in pH values is 0.002.

The variation of pH sensitivity with the waveguide's width and the thickness of the high index layer has been shown in Fig. 10(a) and (b) respectively, along with the propagation loss. The sensitivity is found to be increasing as the width of the waveguide is reduced but at the cost of increased propagation loss. As the width is reduced the modal effective index also decreases, resulting in a higher evanescent field in the pH-sensitive layer. However, as the width is reduced the modal power in

TABLE I
COMPARISON OF THE PROPOSED STRUCTURE WITH THE EARLIER REPORTED RESULTS

Ref.	Sensitivity (nm/pH)	Measurement range (pH)	Operating Principle
[14]	0.052	6-12	Bragg grating
[15]	0.03-0.082	2-12	Tilted Bragg grating
[16]	0.073	4-7	Microstructure Bragg grating
[17]	0.265	4-12	Microfiber Bragg grating
[9]	3.42	1-7	SMF-No core fiber-SMF
[10]	11	4.1-6.9	SMF-hollow core photonic crystal fiber-SMF
[8]	0.66	2-12	LPFG
[11]	28.3	4-7	Mode transition LPFG
[20]	1-18	4-7	Surface plasmon resonance
Proposed structure	10.4	4-7	Bragg grating

the metal layer also starts increasing, causing an increase in propagation loss. The sensitivity is also found to be increasing with the decrement in high index layer thickness up to a certain value (around 30 nm) and then start reducing. It should be noted that the propagation losses start to increase quite sharply after a thickness of around 30 nm which can be attributed to modal hybridization [25].

A comparison has been tabulated with the previously reported sensitivity and pH range in Table I. The table shows that the sensitivity of the proposed device is much higher among all the reported results with Bragg gratings. The reported sensitivity is comparable with the modal interferometer-based structures [9], [10]. However, unlike interferometer-based structures the proposed structure is free from FSR and also has narrower spectral bandwidth, facilitating the detection of the spectral shift. The sensitivity of the proposed structure is found to be lower than the long-period fiber grating (LPFG) based structure operating in the mode transition region. Near mode transition, although the sensitivity is high, it is difficult to achieve good stability in the transmitted spectrum with respect to changes in the analyte. As reported in [11], although the transmittance is good from pH value 7 to 6, it starts to degrade quite sharply as the pH value decreases further. The stability of the spectrum of the proposed structure is better in the entire pH range, which gives it an edge over the mode transition-assisted LPFG structure. Moreover, the proposed structure shows high sensitivity with the quasi-TE mode which has much lower propagation loss as compared to TM modes used in surface plasmon resonance (SPR) based sensors. This can be helpful in overcoming the problems with the signal-to-noise ratio that usually the SPR-based sensors suffer from [31]. Overall, the proposed structure shows good performance over the reported pH sensors in optical fiber/waveguide geometry, implying significant development toward measuring and monitoring pH levels in different fields, especially in the perishable food industry. High pH sensitivity in the pH range of 4 to 7 is highly desirable for the perishable food industry. It has been observed that the acidity level of the foods (especially the perishable ones, which are not fresh) plays an important role in deciding the freshness of the foods since over time the growth of microbial organisms in the foods increases their acidity level. Considering that the pH values below the neutral

value of 7 decide the acidity level, a highly sensitive and accurate sensor is highly recommended for the aforementioned pH range. Moreover, the miniaturized size of the proposed structure along with its high sensitivity, narrow bandwidth, and stable spectrum response with respect to changes in pH values can lead to a promising development toward smart packaging.

B. Possible Way of Fabrication and Fabrication Tolerances

For the practical realization of a sensor structure, it is important to study a possible way of fabrication as well as its fabrication tolerances with respect to various structural parameters. A possible way of fabricating the proposed structure is discussed below sequentially. First, a metallic layer of silver can be deposited on a silica substrate with the sputtering technique [32]. In order to enhance the adhesion between the silica and silver, a monolayer of 3-aminopropyl trimethoxysilane (APTMS) can be used [33]. Next, a 1.5 μm thick layer of PMMA can be spin-coated on top of the metal layer [34]. The advantage of using PMMA as the core is it shows good adhesion with the metal layer as well as can directly act as the photoresist during lithography. The e-beam lithography or deep-UV lithography can be used to form the ridge shape with the desired width of 1.5 μm [34]. In order to investigate the effect of any inaccuracy in the PMMA core's width and height, the peak reflectivity and sensitivity have been calculated considering $\pm 10\%$ errors in both parameters. Hardly any variation in peak reflectivity has been observed with both the parameters as the deviation in peak reflectivity is within 0.85% from the nominal peak reflectivity of 0.7. The deviation in sensitivity is found to be within 3.4% and 2.5% from the nominal sensitivity of 10.4 nm/pH, for $\pm 10\%$ errors in width and height respectively, reflecting an excellent fabrication tolerance. The grating can be formed by periodic exposure to UV radiation with the help of a phase mask [35], [36]. The refractive index of the exposed area of PMMA will be modulated since it is photosensitive to UV radiation whereas the unexposed area will remain the same, creating the periodic modulation of the PMMA core refractive index and forming the grating. In the next step of fabrication, the high index layer of TiO_2 can be deposited using the sputtering technique [37]. Coating the entire structure with TiO_2 also ensures the protection of the silver layer from oxidization. The deviation in peak reflectivity and sensitivity is found to be within 3% for a $\pm 10\%$ error in high index layer thickness, again reflecting good fabrication tolerances of the proposed structure. Finally, the pH-sensitive layer of PAA/PAH can be formed using the electrostatic self-assembling technique [11], [27].

V. CONCLUSION

We propose a compact and highly sensitive pH optical sensor based on polymer waveguide Bragg grating. The high sensitivity has been calculated for the TE mode of the structure in which metal under cladding and a high index nano-coating have been used to respectively push and pull the guided mode towards the surrounding medium. As a result, a high modal power ($\sim 40\%$) has been obtained to interact with a pH-sensitive polymeric nano-coating of the PAA/PAH layer. The pH sensitivity has been numerically investigated following the shrinkage of the

polymeric coating as the pH level changes from 4 to 7. The sensitivity is found to be 10.4 nm/pH, the highest among all the previously reported Bragg grating-based structures to the best of our knowledge. Further, a narrow bandwidth of ~ 1 nm of the reflected spectrum facilitates the detection mechanism. The overall device length is found to be only 0.9 mm. The proposed structure features a great fabrication tolerance as the variation in sensitivity and peak reflectivity is only within 3% for an $\pm 10\%$ inaccuracy in structural parameters. The proposed sensor is free from FSR and also has narrower spectral bandwidth and is particularly an excellent choice for measuring and monitoring the acidity level of perishable foods and smart packaging.

REFERENCES

- [1] D. Wenzel, T. Abel, and C. McDonagh, "Optical chemical pH sensors," *Anal. Chem.*, vol. 86, pp. 15–29, 2014, doi: [10.1021/ac4035168](https://doi.org/10.1021/ac4035168).
- [2] Q. Luo et al., "Recent advances in the fabrication of pH-sensitive indicators films and their application for food quality evaluation," *Crit. Rev. Food Sci. Nutr.*, vol. 63, pp. 1–17, 2021, doi: [10.1080/10408398.2021.1959296](https://doi.org/10.1080/10408398.2021.1959296).
- [3] A. Steinegger, O. S. Wolfbeis, and S. M. Borisov, "Optical sensing and imaging of pH values: Spectroscopies, materials, and applications," *Chem. Rev.*, vol. 120, pp. 12357–12489, 2020, doi: [10.1021/acs.chemrev.0c00451](https://doi.org/10.1021/acs.chemrev.0c00451).
- [4] B. Panda, R. Balasubramaniam, S. Mahapatra, and G. Dwivedi, "Fretting and fretting corrosion behavior of novel micro alloyed rail steels," *Wear*, vol. 267, pp. 1702–1708, 2009, doi: [10.1016/j.wear.2009.06.035](https://doi.org/10.1016/j.wear.2009.06.035).
- [5] H. Lehmann, G. Schwotzer, P. Czerney, and G. J. Mohr, "Fiber-optic pH meter using NIR dye," *Sens. Actuators B Chem.*, vol. 29, pp. 392–400, 1995, doi: [10.1016/0925-4005\(95\)01713-5](https://doi.org/10.1016/0925-4005(95)01713-5).
- [6] J. Goicoechea, C. R. Zamarreño, I. R. Matias, and F. J. Arregui, "Optical fiber pH sensors based on layer-by-layer electrostatic self-assembled Neutral Red," *Sensors Actuators B Chem.*, vol. 132, pp. 305–311, 2008, doi: [10.1016/j.snb.2008.01.056](https://doi.org/10.1016/j.snb.2008.01.056).
- [7] A. K. Pathak and V. K. Singh, "A wide range and highly sensitive optical fiber pH sensor using polyacrylamide hydrogel," *Opt. Fiber Technol.*, vol. 39, pp. 43–48, 2017, doi: [10.1364/AO.415977](https://doi.org/10.1364/AO.415977).
- [8] S.K. Mishra, B. Zou, and K.S. Chiang, "Wide-range pH sensor based on a smart-hydrogel-coated long-period fiber grating," *IEEE J. Sel. Top. Quantum Electron.*, vol. 23, no. 2, pp. 284–288, Mar./Apr. 2017, doi: [10.1109/JSTQE.2016.2629662](https://doi.org/10.1109/JSTQE.2016.2629662).
- [9] T. A. Abdzaid and H. J. Taher, "No-core fiber interferometry pH sensor based on a polyvinyl alcohol polyacrylic acid and silica polyvinyl alcohol polyacrylic acid hydrogel coating," *Appl. Opt.*, vol. 60, pp. 1587–1594, 2021, doi: [10.1364/AO.415977](https://doi.org/10.1364/AO.415977).
- [10] Y. Zheng et al., "Miniature pH optical Fiber sensor based on Fabry–Perot interferometer," *IEEE J. Sel. Top. Quantum Electron.*, vol. 22, no. 2, Mar./Apr. 2016, Art. no. 5600205, doi: [10.1364/AO.410974](https://doi.org/10.1364/AO.410974).
- [11] J. M. Corres, I. R. Matias, I. d. Villar, and F. J. Arregui, "Design of pH sensors in long-period Fiber gratings using polymeric nanocoatings," *IEEE Sens. J.*, vol. 7, no. 3, pp. 455–463, Mar. 2007, doi: [10.1109/JSEN.2007.891933](https://doi.org/10.1109/JSEN.2007.891933).
- [12] P. Zubiarte, C. R. Zamarreño, I. D. Villar, I. R. Matias, and F. J. Arregui, "Tunable optical fiber pH sensors based on TE and TM lossy mode resonances (LMRs)," *Sensors Actuators B Chem.*, vol. 231, pp. 484–449, 2016, doi: [10.1016/j.snb.2016.03.024](https://doi.org/10.1016/j.snb.2016.03.024).
- [13] C. R. Zamarreño, M. Hernáez, I. D. Villar, I. R. Matias, and F. J. Arregui, "Optical fiber pH sensor based on lossy-mode resonances by means of thin polymeric coatings," *Sensors Actuators B Chem.*, vol. 155, pp. 290–297, 2011, doi: [10.1364/AO.51.004298](https://doi.org/10.1364/AO.51.004298).
- [14] X. Liang, S. Chen, H. Huang, and W. Liu, "Study on sensitivity improving of fiber Bragg grating based pH sensor," *Photonic Sensors*, vol. 4, pp. 28–33, 2014, doi: [10.1007/s13320-013-0124-5](https://doi.org/10.1007/s13320-013-0124-5).
- [15] A. L. Aldaba, Á. G. Vila, M. Debliquy, M. L. Amo, C. Caucheteur, and D. Lahem, "Polyaniline-coated tilted fiber Bragg gratings for pH sensing," *Sensors Actuators B Chem.*, vol. 254, pp. 1087–1093, 2018, doi: [10.1016/j.snb.2017.07.167](https://doi.org/10.1016/j.snb.2017.07.167).
- [16] J. Janting, J. K. M. Pedersen, G. Woyessa, K. Nielsen, and O. Bang, "Small and robust all-polymer Fiber Bragg grating based pH sensor," *J. Light. Technol.*, vol. 37, pp. 4480–4486, 2019, doi: [10.1109/JLT.2019.2902638](https://doi.org/10.1109/JLT.2019.2902638).
- [17] Y. Ran et al., "A miniature pH probe using functional microfiber Bragg grating," *Optics*, vol. 1, pp. 202–2012, 2020, doi: [10.3390/opt1020016](https://doi.org/10.3390/opt1020016).
- [18] G. Ren et al., "An ultrasensitive silicon photonic ion sensor enabled by 2D plasmonic molybdenum oxide," *Small*, vol. 15, 2019, Art. no. 1805251, doi: [10.1002/sml.201805251](https://doi.org/10.1002/sml.201805251).
- [19] S. Singh and B. D. Gupta, "Fabrication and characterization of a highly sensitive surface plasmon resonance based fiber optic pH sensor utilizing high index layer and smart hydrogel," *Sensors Actuators B Chem.*, vol. 173, pp. 268–273, 2012, doi: [10.1016/j.snb.2012.06.089](https://doi.org/10.1016/j.snb.2012.06.089).
- [20] S. K. Mishra and B. D. Gupta, "Surface plasmon resonance based fiber optic pH sensor utilizing Ag/ITO/Al/hydrogel layers," *Analyst*, vol. 138, pp. 2640–2646, 2013, doi: [10.1039/C3AN00097D](https://doi.org/10.1039/C3AN00097D).
- [21] H. Li et al., "Silicon-photonics-based waveguide Bragg grating sensor for blood glucose monitoring," *Opt. Exp.*, vol. 30, pp. 41554–41566, 2022, doi: [10.1364/OE.472137](https://doi.org/10.1364/OE.472137).
- [22] N. Saha, A. Kumar, and A. Mukherjee, "Enhancement of refractive index sensitivity of Bragg-gratings based optical waveguide sensors using a metal under-cladding," *Opt. Commun.*, vol. 396, pp. 83–87, 2017, doi: [10.1016/j.optcom.2017.03.043](https://doi.org/10.1016/j.optcom.2017.03.043).
- [23] R. Dwivedi and A. Kumar, "A compact and ultra high sensitive RI sensor using modal interference in an integrated optic waveguide with metal under-cladding," *Sensors Actuators B Chem.*, vol. 240, pp. 1302–1307, 2017, doi: [10.1016/j.snb.2016.09.103](https://doi.org/10.1016/j.snb.2016.09.103).
- [24] N. Saha and A. Kumar, "Toward 100 micrometer per refractive index unit sensitive sensor using a compact long-period grating inscribed metal clad ridge waveguide," *J. Light. Technol.*, vol. 36, no. 10, pp. 2024–2030, May 2018, doi: [10.1109/JLT.2018.2802705](https://doi.org/10.1109/JLT.2018.2802705).
- [25] N. Saha, G. Brunetti, A. Kumar, M.N. Armenise, and C. Ciminelli, "Highly sensitive refractive index sensor based on polymer Bragg grating: A case study on extracellular vesicles detection," *Biosensors*, vol. 12, 2022, Art. no. 415, doi: [10.3390/bios12060415](https://doi.org/10.3390/bios12060415).
- [26] C. P. Armenta et al., "Narrowband Bragg filters based on subwavelength grating waveguides for silicon photonic sensing," *Opt. Exp.*, vol. 28, pp. 37971–37985, 2020, doi: [10.1364/OE.404364](https://doi.org/10.1364/OE.404364).
- [27] J. M. Corres, I. D. Villar, I. R. Matias, and F. J. Arregui, "Fiber-optic pH-sensors in long-period fiber gratings using electrostatic self-assembly," *Opt. Lett.*, vol. 32, pp. 29–31, 2007, doi: [10.1364/OE.26.014610](https://doi.org/10.1364/OE.26.014610).
- [28] G. Beadie, M. Brindza, R. A. Flynn, A. Rosenberg, and J. S. Shirk, "Refractive index measurements of poly(methyl methacrylate) (PMMA) from 0.4–1.6 μm ," *Appl. Opt.*, vol. 54, pp. F139–F143, 2015, doi: [10.1364/AO.54.00F139](https://doi.org/10.1364/AO.54.00F139).
- [29] C.C. Evans, "Nonlinear optics in titanium dioxide: From bulk to integrated optical devices," Ph.D. Dissertation, Harvard Univ., Cambridge, MA, USA, 2013.
- [30] A. Kumar Jitender, R. K. Varshney, and M. Kumar, "Calculation of propagation characteristics of surface plasmons in gold/silver nanowires," *Appl. Opt.*, vol. 54, pp. 3715–3719, 2015, doi: [10.1364/AO.54.003715](https://doi.org/10.1364/AO.54.003715).
- [31] X. Li et al., "Label-free optofluidic nanobiosensor enables real-time analysis of single-cell cytokine secretion," *Small*, vol. 14, 2018, Art. no. 1800698, doi: [10.1021/acssensors.0c01774](https://doi.org/10.1021/acssensors.0c01774).
- [32] N. Marechal, E. Quesnel, and Y. Pauleau, "Silver thin films deposited by magnetron sputtering," *Thin Solid Films*, vol. 241, pp. 34–38, 1994, doi: [10.1016/0040-6090\(94\)90391-3](https://doi.org/10.1016/0040-6090(94)90391-3).
- [33] J. Sukham, O. Takayama, A. V. Lavrinenko, and R. Malureanu, "High quality ultrathin gold layers with an APTMS adhesion for optimal performance of surface plasmon polariton-based devices," *ACS Appl. Mater. Interfaces*, vol. 9, pp. 25049–25056, 2017, doi: [10.1021/acsmi.7b07181](https://doi.org/10.1021/acsmi.7b07181).
- [34] A. Kumar et al., "Dielectric-loaded plasmonic waveguide components: Going practical," *Laser Photon. Rev.*, vol. 7, pp. 938–951, 2013, doi: [10.1002/lpor.201200113](https://doi.org/10.1002/lpor.201200113).
- [35] I. L. Bundalo, K. Nielsen, C. Markos, and O. Bang, "Bragg grating writing in PMMA microstructured polymer optical fibers in less than 7 min," *Opt. Exp.*, vol. 22, pp. 5270–5276, 2014, doi: [10.1364/OE.22.005270](https://doi.org/10.1364/OE.22.005270).
- [36] M. Rosenberger, G. Koller, S. Belle, B. Schmauss, and R. Hellmann, "Planar Bragg grating in bulk polymethylmethacrylate," *Opt. Exp.*, vol. 20, pp. 27288–27296, 2012, doi: [10.1364/OE.20.027288](https://doi.org/10.1364/OE.20.027288).
- [37] M. Rosenberger et al., "TiO₂ surface functionalization of COC based planar waveguide bragg gratings for refractive index sensing," *J. Opt.*, vol. 20, 2018, Art. no. 01LT02, doi: [10.1088/2040-8986/aa9bcf](https://doi.org/10.1088/2040-8986/aa9bcf).